Laser and Particle Beams (2012), *30*, 75–86.

doi:10.1017/S026303461100070X

Analytical and numerical investigation of the pulse-shape effect on the longitudinal electric field of a tightly focused ultrafast few-cycle TM_{01} laser beam

HARISH MALAV,[1] K.P. MAHESHWARI,[1] AND Y. CHOYAL[2]

[1]DST-Project, Vardhaman Mahaveer Open University, Kota, India
[2]School of Physics, Devi Ahilya Vishwavidyalaya, Indore, India

(RECEIVED 27 August 2011; ACCEPTED 22 October 2011)

Abstract

The effect of temporal pulse-shape on the characterization of the longitudinal electric field resulting from the tight-focusing of an ultrashort few-cycle TM_{01} laser beam in free space is investigated analytically and numerically. The longitudinal field is found to be sensitive to the pulse-shape of the driving field. The temporal pulse-shapes considered are Gaussian, Lorentzian, and hyperbolic secant having identical full width at half maximum of intensity. Analytical calculations are made beyond the paraxial and slowly varying envelope approximations. From the numerical results we find that due to finite duration of the signal, the evolution of the pulse envelope before the waist is faster (negative time-delay) but slowed down (positive time-delay) after the waist. This time-delay, for single-cycle pulses of wavelength λ_0, and for spot-size w_{0f} in the range $0.6\lambda_0 > w_{0f} > 0.25\lambda_0$, is pulse-shape dependent. The time delay is maximum for the Gaussian pulse and minimum for the Lorentzian pulse. The carrier frequency shift depends on the temporal profile of the pulse, beam spot size, axial propagating distance and also on the number of cycles in a pulse. In addition, a comparative study of the variation of the corrected axial Gouy- phase of the longitudinal electric field of single-cycle pulse (spot size $w_{0f} = 0.5\lambda_0$) with normalized retarded time shows that the phase variation is maximum for Gaussian and minimum for the Lorentzian pulse shape.

Keywords: Axial Gouy phase; Carrier frequency shift; Laser pulse-shape; Tightly focused TM_{01} laser beam

1. INTRODUCTION

The recent progress in the technologies leading to the generation (Schenkel *et al.*, 2003), phase-measurement (Paulus *et al.*, 2003; Kröll *et al.*, 2007; Wittmann *et al.*, 2009), and control of the sub-cycle evolution (Apolonski *et al.*, 2000) of few-cycle light wave has opened the door to the observations of atomic-scale electron dynamics (Krausz & Ivanov, 2009), electron acceleration (Sprangle *et al.*, 2000; Varin & Piché, 2002; Varin *et al.*, 2005; Esarey *et al.*, 2009; Malav *et al.*, 2011*a*) and high-order harmonic generation (Lichters *et al.*,1996; Villoresi *et al.*, 2001; Baeva *et al.*, 2006; Dromey *et al.*, 2007, 2009; Gupta *et al.*, 2007; Corkum & Krausz 2007; Varro, 2007; Malav *et al.*, 2011*b*). These physical processes are dependent on the electric field, rather than just the intensity envelope of a pulse (Varin & Piché, 2002). Recent experimental results show that a radially polarized field can be focused to a spot size significantly smaller ($0.16\lambda_0^2$) than for linear polarization ($0.26\lambda_0^2$) (Dorn *et al.*, 2003). The effect of the vector properties of light is shown by a comparison of the focal intensity distribution for radially and azimuthally polarized input laser-fields. For strong focusing, a radially polarized field leads to a longitudinal electric field component at the focus which is sharp and centered at the optical axis. Since such laser fields consist of merely a few field oscillations, therefore, the actual time variation of the electric field affects all physical processes driven by the laser. Consequently, the physical processes such as high-harmonic generation, intense laser-matter interaction, diffraction effects etc., depend on the phase of the carrier wave with respect to the envelope, the so called carrier envelope phase (Porras, 2002, 2009; Nisoli *et al.*, 2003). Attention is therefore being paid to the characterization of the axial longitudinal electric field of tightly focused few-cycle pulses in free space.

Address correspondence and reprint requests to: K.P. Maheshwari, DST-Project, Vardhaman Mahaveer Open University, Rawatbhata road, Kota-324010, India. E-mail: malavh@yahoo.co.in

Our main concern in this work is to investigate the pulse-shape effect on the characterization of the axial longitudinal electric field resulting from the tight focusing of an ultrashort few-cycle TM_{01} laser beam in free space. The temporal pulse-shape effects due to ultrashort pulse duration may have important implications for several applications such as acceleration of charge particles (Malav *et al.*, 2011*a*), high order harmonic generation (Malav *et al.*, 2011*b*). The present numerical study extends the work by Varin *et al.* (2006) that includes the effect of temporal profile of the incident laser pulse on the characterization of the longitudinal electric field.

Following Brabec and Krausz (1997), we express the temporal form of the pulsed beam as enveloped carrier oscillations of the averaged carrier frequency ω_0. The temporal pulse-shapes considered are Gaussian, Lorentzian, and hyperbolic secant having identical full-width at half maximum of intensity. Using a complete vectorial description of an ultrafast tightly focused TM_{01} laser beam in free space having different temporal pulse-shapes, analytical expressions beyond the paraxial and slowly varying envelope approximations are obtained for longitudinal electric field. The results show that due to the finite duration of the signal, the evolution of the pulse envelope before the waist is faster (negative time-delay) but slowed down (positive time-delay) after the waist, and this time-delay is pulse-shape dependent for single-cycle pulses having spot-size in the range $0.6\lambda_0 > w_{0f} > 0.25\lambda_0$. The magnitude of the time delay is maximum for the Gaussian pulse- shape and minimum for the Lorentzian pulse-shape. With smaller spot size, the laser beam divergence is faster than predicted by the paraxial theory. There is also a carrier-frequency- shift that depends on the pulse-shape, beam spot-size, axial propagating distance, and also on the number of cycles in a pulse. It is also found that there is a faster evolution of the axial Gouy phase shift in the vicinity of the focus that depends on the pulse-shape. However, the Gouy phase at the Rayleigh range for single-cycle tightly focused laser beam does not depend on the pulse shape.

The work is organized as follows: In Section 2, we present the field equations of tightly focused ultrafast TM_{01} beam in free space. In Section 3, we present expressions that exhibit the pulse-shape dependence of the axial longitudinal electric field of the tightly focused TM_{01} laser beam in free space. In Section 4, we analyze the results and give discussion. Section 5 presents our conclusions.

2. FIELD EQUATIONS OF TIGHTLY FOCUSED ULTRAFAST TM_{01} BEAM IN FREE SPACE

The electric field vector E of electromagnetic wave in free-space can be expressed as

$$E = \mathrm{Re}\Big[\widetilde{E}\exp\{\, j(\omega_0 t - k_0 z)\}\Big], \tag{1}$$

with $\widetilde{E}$ being the complex envelope of electric field vector, ω_0 is of center carrier frequency and k_0 is free space wave vector. In terms of the reduced variables $t' = t - z/c$, $z' = z$, the vector $\widetilde{E}$ satisfies the perturbed paraxial wave equation (Porras, 2001; Varin *et al.*, 2006):

$$\nabla_\perp^2 \widetilde{E} - 2j k_0 \partial_{z'} [1 - \Theta]\widetilde{E} = 0, \tag{2}$$

with

$$\Theta = j\{\omega_0^{-1}\partial_{t'} - (2k_0)^{-1}\partial_{z'}\}. \tag{3}$$

A solution to perturbed paraxial wave equation can be found by expanding the envelope of the electric field vector as a power series. The complex envelope of the longitudinal electric field E_z can be expressed as:

$$\widetilde{E}_z = \sum_{m=0}^{\infty}\sum_{n=0}^{\infty} j^{m+n}\left(\frac{\partial_{t'}}{\omega_0} - \frac{\partial_{z'}}{k_0}\right)^m \times \left(\frac{\partial_{t'}}{\omega_0} - \frac{\partial_{z'}}{2k_0}\right)^n \times \partial_{z'}^{n-1}\left(\frac{z'^n}{n!}\partial_{z'}\widetilde{E}_z^{(0)}\right), \tag{4}$$

where $\widetilde{E}_z^{(0)}$ is the paraxial and slowly varying envelope of the longitudinal electric field.

Higher order terms follow from elemental operations on the zeroth order solution. These are the corrections up to the order of $(1/\omega_0\tau)^n(1/k_0 z_{Rf})^m$ for $n, m \geq 1$, are expected to decrease with growing n and m for $1/\omega_0\tau < 1$, $1/k_0 z_{Rf} < 1$.

Here, we consider the case of an ultrafast TM_{01} beam ($B_z = B_r = E_\theta = 0$) that is tightly focused by an ideal lens free of all aberrations.

The waist of the entrance beam E^i is at $z' = 0$. A lens of focal length f is placed at $z' = z_1$. The waist of the output beam E^f is located at $z' = z_f$ (Fig. 1 of Varin *et al.*, 2006).

The paraxial and slowly varying envelope of the longitudinal electric field after the lens can be expressed as

$$\widetilde{E}_z^{f(0)} = -\frac{2\sqrt{2}jE_{0f}}{k_0 w_{0f}}\exp(1/2)\left(\frac{jz_{Rf}}{\widetilde{q}_f}\right)^2\left(1 - \frac{jk_0 r^2}{2\widetilde{q}_f}\right) \times \exp\left(-\frac{jk_0 r^2}{2\widetilde{q}_f}\right)A_f(t'), \tag{5}$$

where E_{0f} is the amplitude of the transverse field after the lens, $\widetilde{q}_f = \Delta z' + jz_{Rf} = z' - z_f + jz_{Rf}$ is the complex parameter of the Gaussian beam, $z_{Rf} = \frac{k_0 w_{0f}^2}{2}$ is the Rayleigh distance, w_{0f} is the beam-spot-size at the waist and $A_f(t')$ is the temporal profile of the pulse envelope after the lens.

The temporal profiles of the envelopes for a Gaussian, Lorentzian, and hyperbolic secant pulses are taken to be (Brabec & Krausz, 2000)

$$A_{fg}(t') = \exp\left[-\left(\frac{1.17t'}{\tau}\right)^2\right], \tag{6.1}$$

https://doi.org/10.1017/S026303461100070X Published online by Cambridge University Press

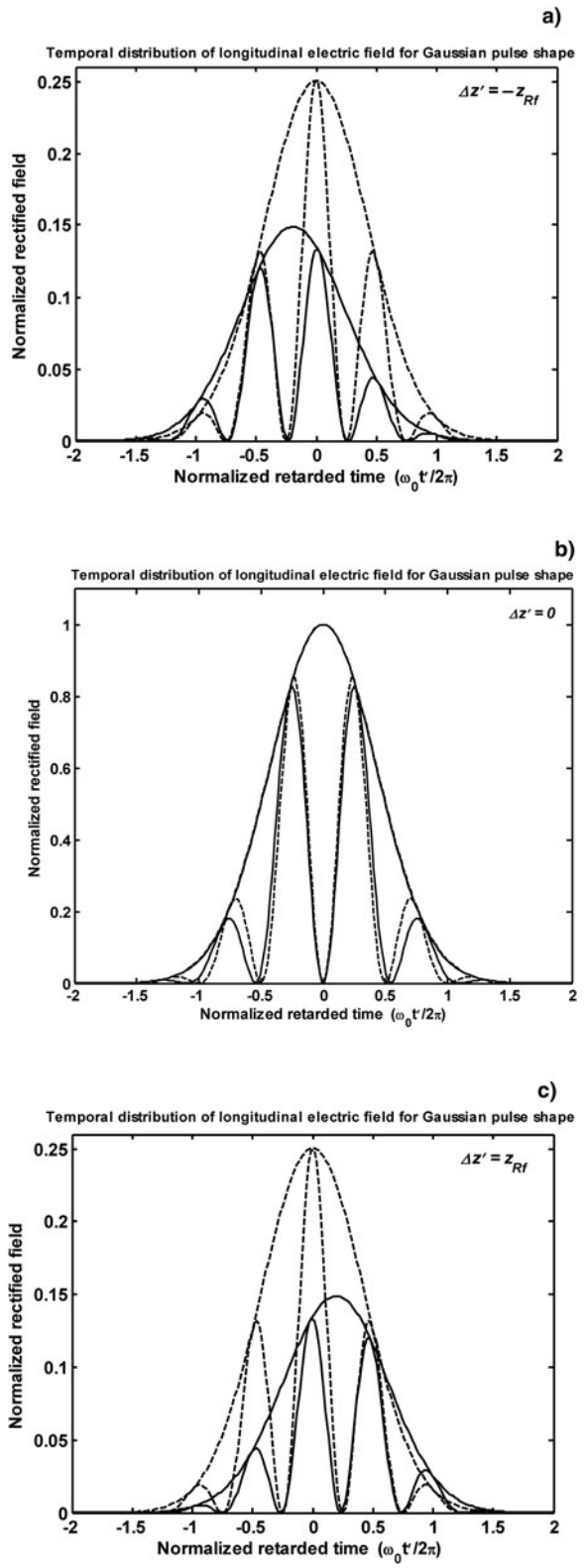

Fig. 1. Shows the temporal distribution of on-axis longitudinal electric field of a ultrafast, single cycle tightly focused laser beam (beam spot-size $w_{0f} = \lambda_0$) having Gaussian pulse-shape at (**a**) for $\Delta z' = -z_{Rf}$, (**b**) $\Delta z' = 0$, and (**c**) $\Delta z' = z_{Rf}$. Bold and dashed lines represent the results of paraxial and non-paraxial approximation, respectively. The absolute value of the fields has been normalized so that their envelopes are equal to 1 at the centre of the pulse ($t' = 0$) and at the waist ($\Delta z' = 0$).

$$A_{fl}(t') = \left[1 + \left(\frac{1.29t'}{\tau}\right)^2\right]^{-1}, \tag{6.2}$$

and

$$A_{fh}(t') = \operatorname{sech}\left(\frac{1.76t'}{\tau}\right), \tag{6.3}$$

respectively, where τ is full width at half maximum of pulse intensity.

$\tilde{E}_z$ has been expressed as an infinite series in terms of successive derivatives of zeroth order solution $\tilde{E}_z^{(0)}$. The series expansions are converging for on axis longitudinal electric field of few-cycle ultra-short tightly focused TM_{01} beams in free space for $1/\omega_0\tau < 1$, $1/k_0 z_{Rf} < 1$ (Porras, 2002). The series expansion truncated to second order in temporal and spatial parts contains terms proportional to $1/(k_0 z_{Rf})^2$, $1/(\omega_0\tau)^2$ and $1/\omega_0\tau k_0 z_{Rf}$.

For the single-cycle pulse, the zeroth, first order, second order, third order terms compare as 1 : 0.159: 0.025: 0.004 and for two-cycle pulse, the zeroth, first order, second order, third order terms compare as 1 : 0.079: 0.0061: 0.0005. It is seen that the higher-order terms give insignificant contribution to the field.

3. PULSE-SHAPE DEPENDENCE OF THE AXIAL LONGITUDINAL ELECTRIC FIELD OF THE TIGHTLY FOCUSED TM_{01} LASER BEAM IN FREE SPACE

Following Varin *et al.* (2006), one finds that at the center of the TM_{01} tightly focused pulsed laser beam, the longitudinal electric field reaches its maximum amplitude. When the spot size approaches the wave-length, second order intensity corrections to the paraxial approximation become important.

The second order electric field E_z^f of a few cycle TM_{01} beam at $r = 0$ can be expressed as the real part of the complex envelope times the carrier wave. Thus,

$$E_z^f = \operatorname{Re}\left[\tilde{E}_z^f \exp(j\omega_0 t')\right] = \left|\tilde{E}_z^{f0}\right|\left|\tilde{C}\right| \cos\left[\Phi(\Delta z', t')\right], \tag{7}$$

where $\tilde{E}_z^f = \tilde{E}_z^{f\,0}\tilde{C}$ and $\tilde{E}_z^{f0}$ is axial zeroth order field.

$$\Phi(\Delta z', t') = \omega_0 t' + 2\tan^{-1}\left(\Delta z'/z_{Rf}\right) + \phi_c - \pi/2, \tag{8}$$

is total phase of the longitudinal electric fields, where $\phi_c =$ argument $\tilde{C} = \tan^{-1}\left(\frac{\operatorname{Im}(\tilde{C})}{\operatorname{Re}(\tilde{C})}\right)$. In the following we derive expressions for the second-order on-axis longitudinal electric field of a few-cycle ultrashort tightly focused TM_{01} beam in free space for the different pulse shapes.

Substituting for Gaussian, Lorentzian, and hyperbolic secant temporal profile pulse-shape i.e Eq. (6) in Eq. (5)

https://doi.org/10.1017/S026303461100070X Published online by Cambridge University Press

and using Eq. (4), the field at the focus of the ideal lens is given by the following expressions:

(1) Gaussian pulse-shape

$$\widetilde{E}_z^f = \widetilde{E}_z^{f0}\Bigg[1+\frac{3j}{k_0\widetilde{q}_f}\left(1-\frac{\Delta z'}{\widetilde{q}_f}\right)-\frac{2j(1.17)^2t'}{\omega_0\tau^2} \times\left(1-\frac{2\Delta z'}{\widetilde{q}_f}\right)+\frac{2(1.17)^2}{\omega_0^2\tau^2}\left(1-\frac{2(1.17)^2t'^2}{\tau^2}\right) \times\left(1-4\frac{\Delta z'}{\widetilde{q}_f}+3\frac{\Delta z'^2}{\widetilde{q}_f^{\,2}}\right)+\frac{2(1.17)^2t'}{k_0\widetilde{q}_f\omega_0\tau^2} \times\left(9-21\frac{\Delta z'}{\widetilde{q}_f}+12\frac{\Delta z'^2}{\widetilde{q}_f^{\,2}}\right)+\frac{3}{2\left(k_0\widetilde{q}_f\right)^2} \times\left(-11+20\frac{\Delta z'}{\widetilde{q}_f}-10\frac{\Delta z'^2}{\widetilde{q}_f^{\,2}}\right)\Bigg], \tag{9}$$

where $\widetilde{E}_z^{f0} = -\dfrac{2\sqrt{2}jE_{0f}}{k_0w_{0f}}\exp(1/2)\left(\dfrac{jz_{Rf}}{\widetilde{q}_f}\right)^2 A_{fg}(t')$.

$$\mathrm{Re}(\widetilde{C}) = 1+\frac{4(1.17)^2t'z_0}{\omega_0\tau^2\left(1+z_0^2\right)}+\frac{3\left(1-z_0^2\right)}{k_0z_{Rf}\left(1+z_0^2\right)^2} +\frac{2(1.17)^2\left(1-5z_0^2\right)}{\omega_0^2\tau^2\left(1+z_0^2\right)^2}\left\{1-\frac{2(1.17)^2(t')^2}{\tau^2}\right\} +\frac{2(1.17)^2t'\left(30z_0-18z_0^3\right)}{k_0z_{Rf}\omega_0\tau^2\left(1+z_0^2\right)^3} +\frac{3\left(11-59z_0^2+9z_0^4-z_0^6\right)}{2k_0^2z_{Rf}^2\left(1+z_0^2\right)^4}, \tag{10}$$

where $z_0 = \dfrac{\Delta z'}{z_{Rf}}$.

$$\mathrm{Im}(\widetilde{C}) = \frac{6z_0}{k_0z_{Rf}\left(1+z_0^2\right)^2}-\frac{2(1.17)^2t'\left(1-z_0^2\right)}{\omega_0\tau^2\left(1+z_0^2\right)} +\frac{2(1.17)^2\left(4z_0-2z_0^3\right)}{\omega_0^2\tau^2\left(1+z_0^2\right)^2}\left\{1-\frac{2(1.17)^2(t')^2}{\tau^2}\right\} +\frac{2(1.17)^2t'\left(-9+36z_0^2-3z_0^4\right)}{k_0z_{Rf}\omega_0\tau^2\left(1+z_0^2\right)^3} +\frac{3\left(42z_0-36z_0^3+2z_0^5\right)}{2k_0^2z_{Rf}^2\left(1+z_0^2\right)^4} \tag{11}$$

(2) Lorentzian pulse-shape

$$\widetilde{E}_z^f = \widetilde{E}_z^{f0}\Bigg[1+\frac{3j}{k_0\widetilde{q}_f}\left(1-\frac{\Delta z'}{\widetilde{q}_f}\right)-\frac{2j(1.29)^2t'A_{fl}}{\omega_0\tau^2} \times\left(1-\frac{2\Delta z'}{\widetilde{q}_f}\right)+\frac{2(1.29)^2A_{fl}}{\omega_0^2\tau^2} \times\left\{1-\frac{4(1.29)^2t'^2A_{fl}}{\tau^2}\right\}\left(1-4\frac{\Delta z'}{\widetilde{q}_f}+3\frac{\Delta z'^2}{\widetilde{q}_f^{\,2}}\right) +\frac{2(1.29)^2t'A_{fl}}{k_0\widetilde{q}_f\omega_0\tau^2}\left(9-21\frac{\Delta z'}{\widetilde{q}_f}+12\frac{\Delta z'^2}{\widetilde{q}_f^{\,2}}\right) +\frac{3}{2\left(k_0\widetilde{q}_f\right)^2}\left(-11+20\frac{\Delta z'}{\widetilde{q}_f}-10\frac{\Delta z'^2}{\widetilde{q}_f^{\,2}}\right)\Bigg], \tag{12}$$

where $\widetilde{E}_z^{f0} = -\dfrac{2\sqrt{2}jE_{0f}}{k_0w_{0f}}\exp(1/2)\left(\dfrac{jz_{Rf}}{\widetilde{q}_f}\right)^2 A_{fl}(t')$.

$$\mathrm{Re}(\widetilde{C}) = 1+\frac{4(1.29)^2tA_{fl}z_0}{\omega_0\tau^2\left(1+z_0^2\right)}+\frac{3(1-z_0^2)}{k_0z_{Rf}(1+z_0^2)^2} +\frac{2(1.29)^2A_{fl}(1-5z_0^2)}{\omega_0^2\tau^2(1+z_0^2)^2}\left\{1-\frac{4(1.29)^2t^2A_{fl}}{\tau^2}\right\} +\frac{2(1.29)^2A_{fl}t(30z_0-18z_0^3)}{k_0z_{Rf}\omega_0\tau^2(1+z_0^2)^3} +\frac{3(11-59z_0^2+9z_0^4-z_0^6)}{2k_0^2Z_R^2(1+z_0^2)^4}, \tag{13}$$

where $z_0 = \dfrac{\Delta z'}{z_{Rf}}$.

$$\mathrm{Im}(\widetilde{C}) = \frac{6z_0}{k_0z_{Rf}(1+z_0^2)^2}-\frac{2(1.29)^2tA_{fl}(1-z_0^2)}{\omega_0\tau^2(1+z_0^2)} +\frac{2(1.29)^2A_{fl}(4z_0-2z_0^3)}{\omega_0^2\tau^2(1+z_0^2)^2}\left\{1-\frac{4(1.29)^2t^2A_{fl}}{\tau^2}\right\} +\frac{2(1.29)^2A_{fl}t(-9+36z_0^2-3z_0^4)}{k_0z_{Rf}\omega_0\tau^2(1+z_0^2)^3} +\frac{3(42z_0-36z_0^3+2z_0^5)}{2k_0^2z_{Rf}^2(1+z_0^2)^4} \tag{14}$$

(3) Hyperbolic secant pulse-shape

$$\widetilde{E}_z^f = \widetilde{E}_z^{f0}\Bigg[1+\frac{3j}{k_0\widetilde{q}_f}\left(1-\frac{\Delta z'}{\widetilde{q}_f}\right)-\frac{j(1.76)\tanh\left(\frac{1.76t'}{\tau}\right)}{\omega_0\tau} \times\left(1-\frac{2\Delta z'}{\widetilde{q}_f}\right)-\frac{(1.76)^2(1-2A_{fh}^2)}{\omega_0^2\tau^2} \times\left(1-4\frac{\Delta z'}{\widetilde{q}_f}+3\frac{\Delta z'^2}{\widetilde{q}_f^{\,2}}\right)+\frac{(1.76)\tanh\left(\frac{1.76t'}{\tau}\right)}{k_0\widetilde{q}_f\omega_0\tau} \times\left(9-21\frac{\Delta z'}{\widetilde{q}_f}+12\frac{\Delta z'^2}{\widetilde{q}_f^{\,2}}\right)+\frac{3}{2(k_0\widetilde{q}_f)^2} \times\left(-11+20\frac{\Delta z'}{\widetilde{q}_f}-10\frac{\Delta z'^2}{\widetilde{q}_f^{\,2}}\right)\Bigg], \tag{15}$$

https://doi.org/10.1017/S026303461100070X Published online by Cambridge University Press

where $\widetilde{E}_z^{f0} = -\dfrac{2\sqrt{2}jE_{0f}}{k_0 w_{0f}} \exp(1/2)\left(\dfrac{jz_{Rf}}{\widetilde{q}_f}\right)^2 A_{fh}(t')$.

$$\mathrm{Re}(\widetilde{C}) = 1 + \frac{2(1.76)z_0 \tanh\left(\frac{1.76t'}{\tau}\right)}{\omega_0\tau(1+z_0^2)} + \frac{3(1-z_0^2)}{k_0 z_{Rf}(1+z_0^2)^2} - \frac{(1.76)^2(1-2A_{fh}^2)(1-5z_0^2)}{\omega_0^2\tau^2(1+z_0^2)^2} + \frac{(1.76)\tanh\left(\frac{1.76t'}{\tau}\right)(30z_0 - 18z_0^3)}{k_0 z_{Rf}\omega_0\tau(1+z_0^2)^3} + \frac{3(11 - 59z_0^2 + 9z_0^4 - z_0^6)}{2k_0^2 Z_R^2(1+z_0^2)^4}, \quad (16)$$

where $z_0 = \dfrac{\Delta z'}{z_{Rf}}$.

$$\mathrm{Im}(\widetilde{C}) = \frac{6z_0}{k_0 z_{Rf}(1+z_0^2)^2} - \frac{(1.76)z_0\tanh\left(\frac{1.76t'}{\tau}\right)(1-z_0^2)}{\omega_0\tau(1+z_0^2)} - \frac{(1.76)^2(1-2A_{fh}^2)(4z_0 - 2z_0^3)}{\omega_0^2\tau^2(1+z_0^2)^2} + \frac{(1.76)\tanh\left(\frac{1.76t'}{\tau}\right)(-9 + 36z_0^2 - 3z_0^4)}{k_0 z_{Rf}\omega_0\tau(1+z_0^2)^3} + \frac{3(42z_0 - 36z_0^3 + 2z_0^5)}{2k_0^2 z_{Rf}^2(1+z_0^2)^4} \quad (17)$$

For a given axial distance we have a phase correction due to the corrected field i.e. $\tilde{C}$, which gives a shift in carrier frequency. The total phase of the field can be expressed as

$$\Phi(\Delta z', t') = \omega_0 t' + 2\tan^{-1}\left(\frac{\Delta z'}{z_{Rf}}\right) + \phi_c - \pi/2 = \omega_0'(\Delta z', t')t' - \frac{\pi}{2}, \quad (18)$$

where $\omega_0' = \omega_0 + \dfrac{\phi_c(0,t')}{t'} + 2(t')^{-1}\tan^{-1}\left(\Delta z'/z_{Rf}\right)$.

The carrier frequency shift can be defined as

$$\Delta\omega = \omega_0'(\Delta z', t') - \omega_0 = \frac{2\tan^{-1}\left(\frac{\Delta z'}{z_{Rf}}\right) + \phi_c}{t'}. \quad (19)$$

Normalized frequency shift at the beam waist can be expressed as:

For Gaussian pulse shape

$$\left(\frac{\omega_0' - \omega_0}{\omega_0}\right)_{\Delta z'=0} = -\frac{1}{\omega_0 t'}\tan^{-1}\left\{\frac{2(1.17)^2 k_g t'}{\omega_0\tau^2}\right\}, \quad (20)$$

where

$$k_g = \frac{1 + \dfrac{9}{k_o z_{Rf}}}{1 + \dfrac{3}{k_o z_{Rf}} + \dfrac{2(1.17)^2}{\omega_0^2\tau^2}\left\{1 - \dfrac{2(1.17)^2(t')^2}{\tau^2}\right\} + \dfrac{33}{2k_0^2 z_{Rf}^2}}. \quad (20.1)$$

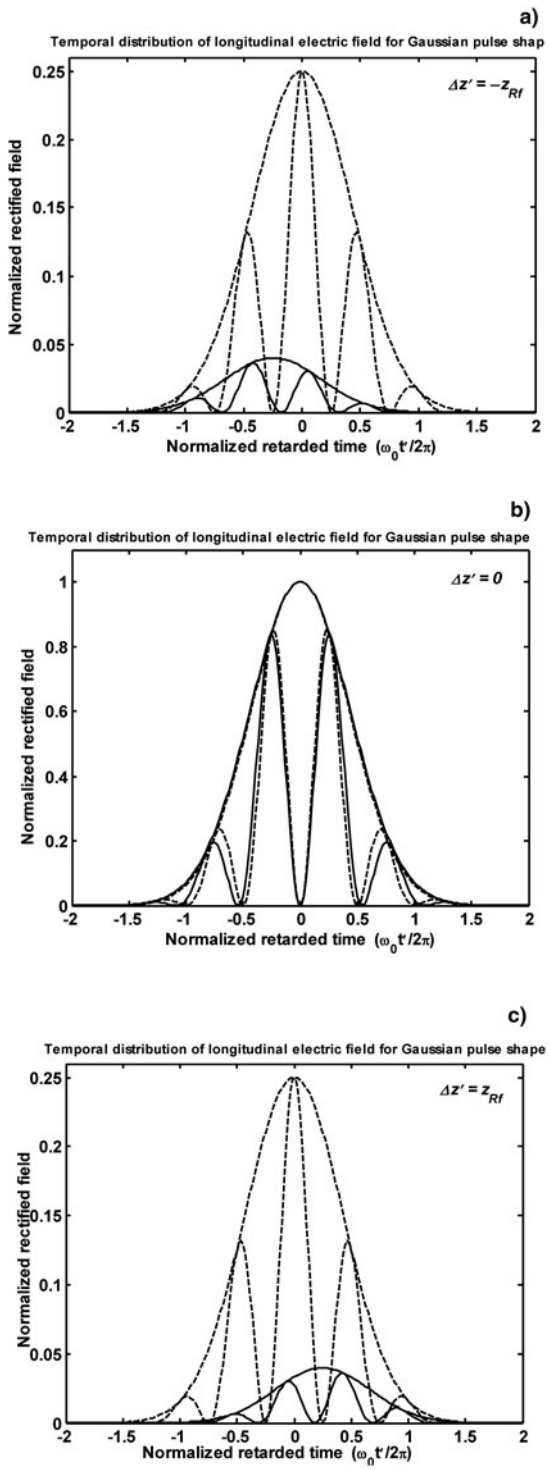

Fig. 2. Shows the temporal distribution of on-axis longitudinal electric field of a ultrafast, single cycle tightly-focused laser beam (beam spot-size $w_{0f} = 0.5\lambda_0$) having Gaussian pulse at (**a**) $\Delta z' = -z_{Rf}$, (**b**) $\Delta z' = 0$, and (**c**) $\Delta z' = z_{Rf}$. Bold and dashed lines represent the results of paraxial and non-paraxial approximation respectively. For normalization see caption of Figure 1.

For Lorentzian pulse shape

$$\left(\frac{\omega_0' - \omega_0}{\omega_0}\right)_{\Delta z'=0} = -\frac{1}{\omega_0 t'}\tan^{-1}\left\{\frac{2(1.29)^2 k_l t' A_{fl}}{\omega_0\tau^2}\right\}, \quad (21)$$

https://doi.org/10.1017/S026303461100070X Published online by Cambridge University Press

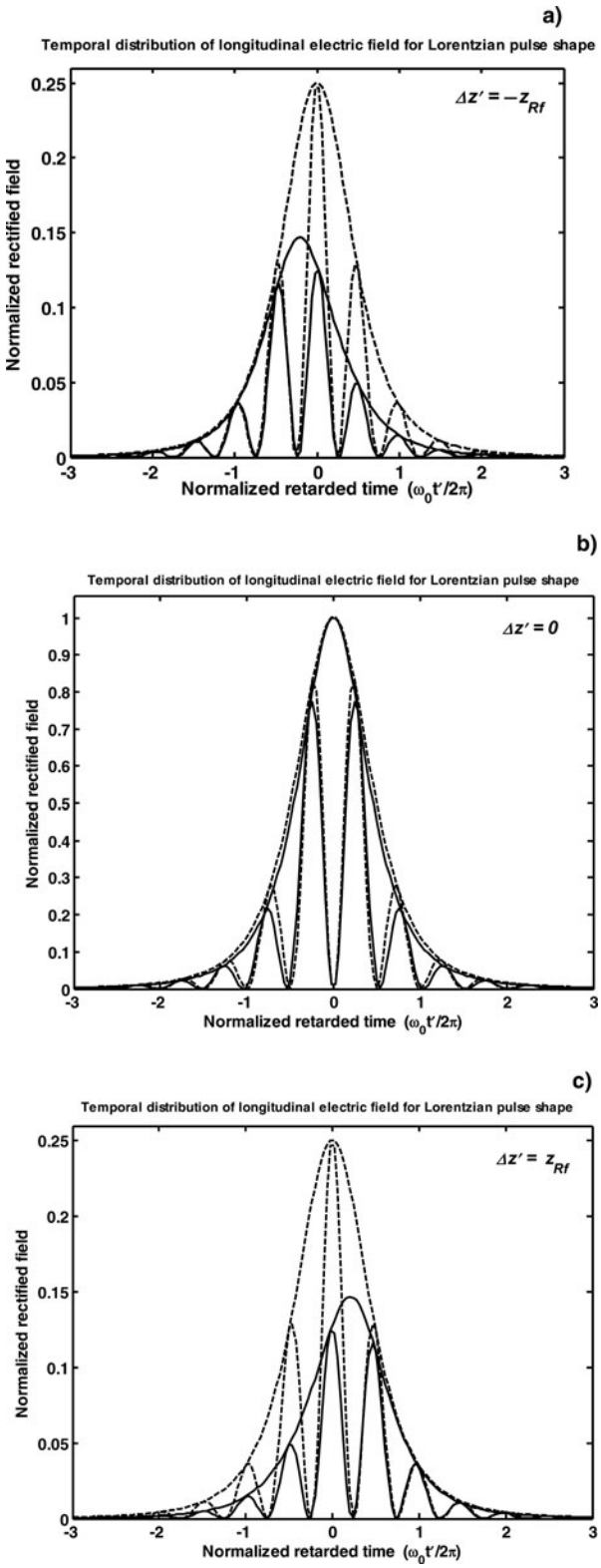

Fig. 3. Shows the temporal distribution of on-axis longitudinal electric field of a ultrafast, single cycle tightly focused beam (beam spot-size $w_{0f} = \lambda_0$) having Lorentzian pulse-shape at (**a**) $\Delta z' = -z_{Rf}$, (**b**) $\Delta z' = 0$, and (**c**) $\Delta z' = z_{Rf}$. Bold and dashed lines represent the results of paraxial and non-paraxial approximation respectively. For normalization see caption of Figure 1.

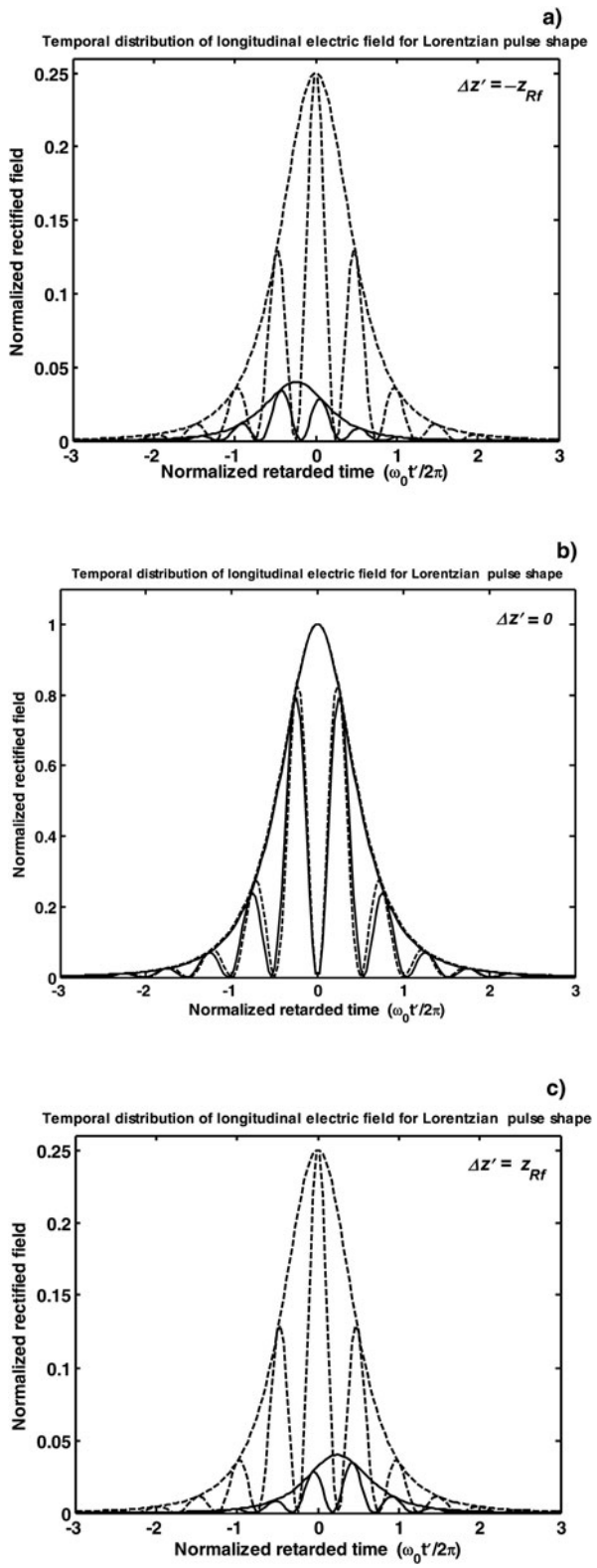

Fig. 4. Shows the temporal distribution of on-axis longitudinal electric field of a ultrafast, single cycle tightly-focused laser beam (beam spot-size $w_{0f} = 0.5\lambda_0$) having Lorentzian pulse at (**a**) $\Delta z' = -z_{Rf}$, (**b**) $\Delta z' = 0$, and (**c**) $\Delta z' = z_{Rf}$. Bold and dashed lines represent the results of paraxial and non-paraxial approximation respectively. For normalization see caption of Figure 1.

https://doi.org/10.1017/S026303461100070X Published online by Cambridge University Press

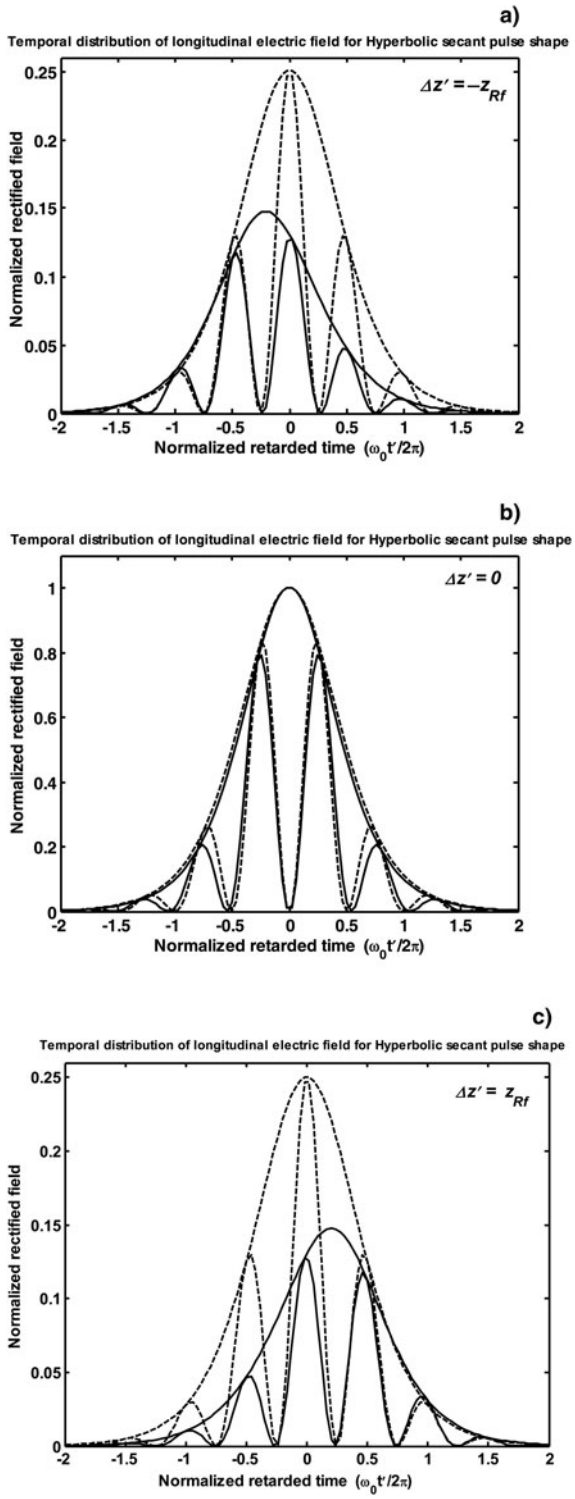

Fig. 5. Shows the temporal distribution of on-axis longitudinal electric field of a ultrafast, single cycle tightly-focused beam (beam spot-size $w_{0f} = \lambda_0$) having hyperbolic secant pulse-shape at (**a**) $\Delta z' = -z_{Rf}$, (**b**) $\Delta z' = 0$, and (**c**) $\Delta z' = z_{Rf}$. Bold and dashed lines represent the results of paraxial and non-paraxial approximation respectively. For normalization see caption of Figure 1.

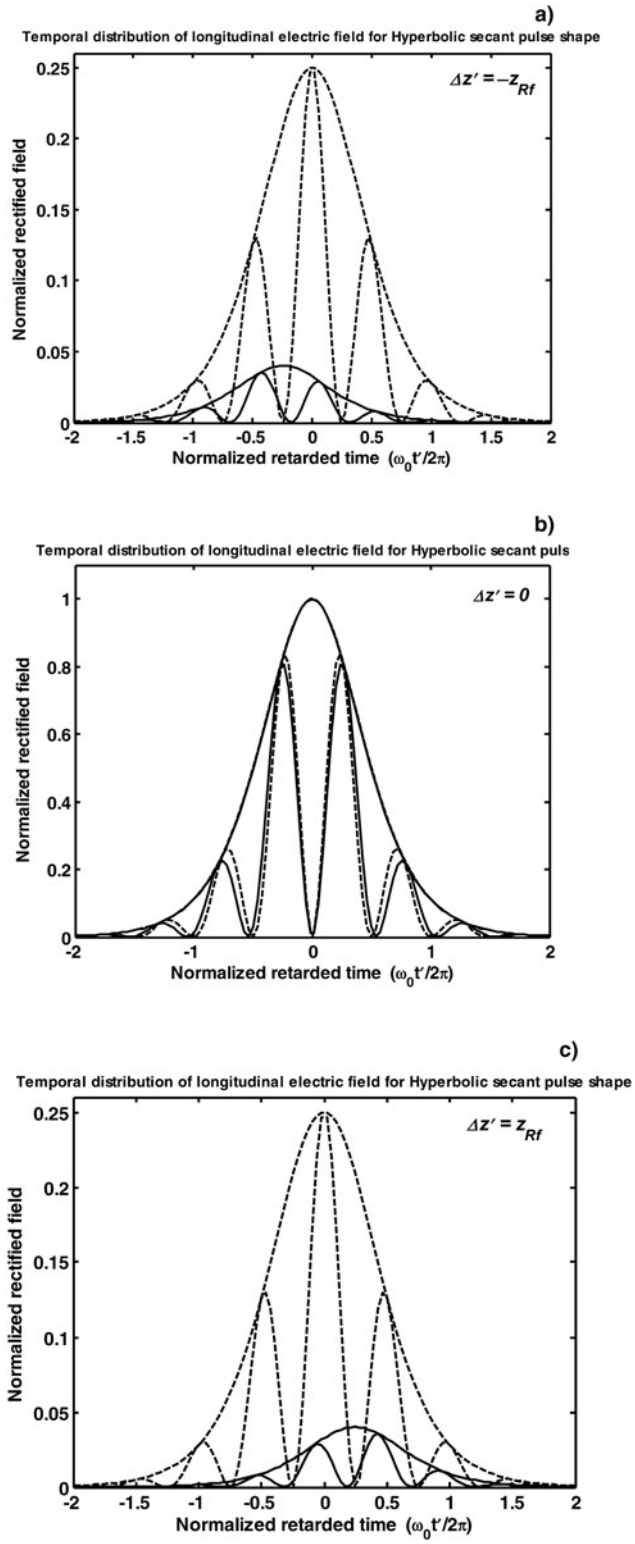

Fig. 6. Shows the temporal distribution of on-axis longitudinal electric field of a ultrafast, single cycle tightly focused beam (beam spot-size $w_{0f} = 0.5\lambda_0$) having hyperbolic secant pulse at (**a**) $\Delta z' = -z_{Rf}$, (**b**) $\Delta z' = 0$, and (**c**) $\Delta z' = z_{Rf}$. Bold and dashed lines represent the results of paraxial and non-paraxial approximation respectively. For normalization see caption of Figure 1.

https://doi.org/10.1017/S026303461100070X Published online by Cambridge University Press

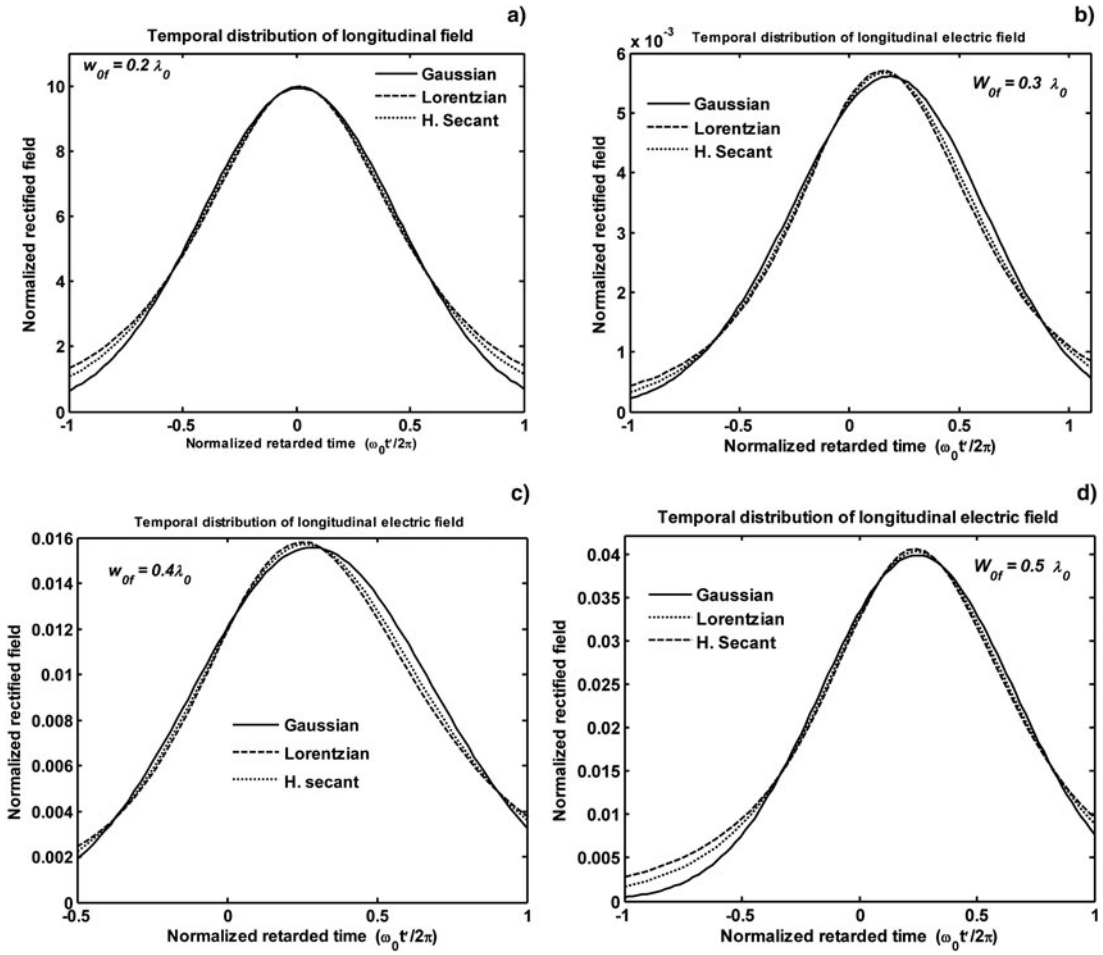

Fig. 7. Shows the temporal distribution of the on-axis longitudinal electric field for different single-cycle pulse envelopes corresponding to different values of the beam spot size at$\Delta z' = z_{Rf}$. The absolute value of the fields have been normalized so that Gaussian envelopes are equal to 1 at $t' = 0$ and $\Delta z' = 0$.

where

$$k_l = \frac{1 + \dfrac{9}{k_o z_{Rf}}}{1 + \dfrac{3}{k_o z_{Rf}} + \dfrac{2(1.29)^2 A_{fl}}{\omega_0^2 \tau^2}\left\{1 - \dfrac{4(1.17)^2 (t')^2 A_{fl}}{\tau^2}\right\} + \dfrac{33}{2k_0^2 z_{Rf}^2}} \tag{21.1}$$

For hyperbolic secant pulse shape

$$\left(\frac{\omega_0' - \omega_0}{\omega_0}\right)_{\Delta z'=0} = -\frac{1}{\omega_0 t'} \tan^{-1} \times \left\{\frac{(1.76) k_s \tanh\left(1.76 t'/\tau\right)}{\omega_0 \tau}\right\}, \tag{22}$$

where

$$k_s = \frac{1 + \dfrac{9}{k_o z_{Rf}}}{1 + \dfrac{3}{k_o z_{Rf}} - \dfrac{(1.76)^2}{\omega_0^2 \tau^2}\left\{1 - 2A_{fh}^2\right\} + \dfrac{33}{2k_0^2 z_{Rf}^2}}. \tag{22.1}$$

and the phase shift is given by

$$\Delta\Phi(\Delta z', t') = \omega_0 t' + 2\tan^{-1}\left(\frac{\Delta z'}{z_{Rf}}\right) + \phi_c. \tag{23}$$

The corrected axial Gouy phase at the centre of the pulse is

$$\phi_{GC} = 2\tan^{-1}\left(\frac{\Delta z'}{z_{Rf}}\right) + \phi_c. \tag{24}$$

4. RESULTS AND DISCUSSION

In Figures 1 and 2, we demonstrate the temporal distribution of the axial longitudinal electric field of a Gaussian laser

https://doi.org/10.1017/S026303461100070X Published online by Cambridge University Press

pulse at various positions along the z' axis for beam spot-size $w_{0f} = \lambda_0$ and $w_{0f} = 0.5\lambda_0$, respectively. The absolute value of the fields has been normalized so that their envelopes are equal to 1 at the center of the pulse ($t' = 0$) and at the waist ($\Delta z' = 0$). The dotted curve is obtained in the paraxial approximation (zeroth –order), while the solid line curve has been obtained incorporating second order fields. We note that the distribution of the field differs from what is expected from the paraxial wave theory. Although pulses emitted from many lasers can be approximated by a Gaussian shape, it is also important to consider the effect of other pulse-shapes viz. Lorentzian and the hyperbolic-secant on the axial longitudinal electric field. Figures 3 and 4, depict the temporal distribution of the longitudinal electric field for a TM_{01} Lorentzian pulse along the z' axis at the beam center for spot size $w_{0f} = \lambda_0$ and $w_{0f} = 0.5\lambda_0$, respectively. Figures 5 and 6, represent the temporal distribution of the longitudinal electric field of a hyperbolic secant laser pulse along the z' axis at the beam centre for spot size $w_{0f} = \lambda_0$ and $w_{0f} = 0.5\lambda_0$, respectively. From these results it is seen that in the non-paraxial approximation the pulse envelope attains its maximum faster as compared to paraxial approximation for $\Delta z' < 0$ and slower for $\Delta z' > 0$. Figure 7 shows the temporal distribution of the longitudinal electric field for different single-cycle pulse shapes at $\Delta z' = z_{Rf}$

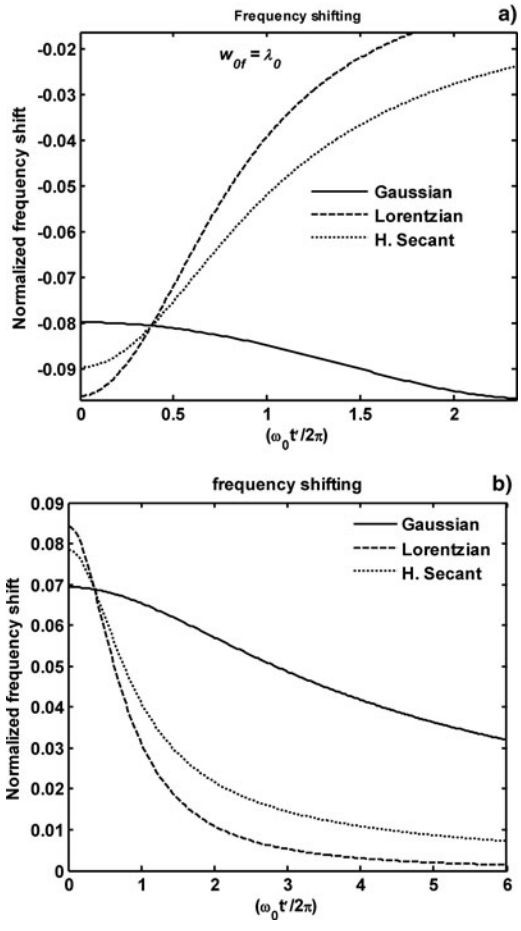

Fig. 8. (**a**) Shows the variation of the axial frequency shift of a single-cycle ultrafast tightly focused TM_{01} beam ($w_{0f} = \lambda_0$) at the beam waist as a function of retarded time. (**b**) Shows the variation of the axial frequency shift of an single-cycle ultrafast tightly focused TM_{01} beam at far from the waist ($\Delta z' = \infty$) as a function of retarded time.

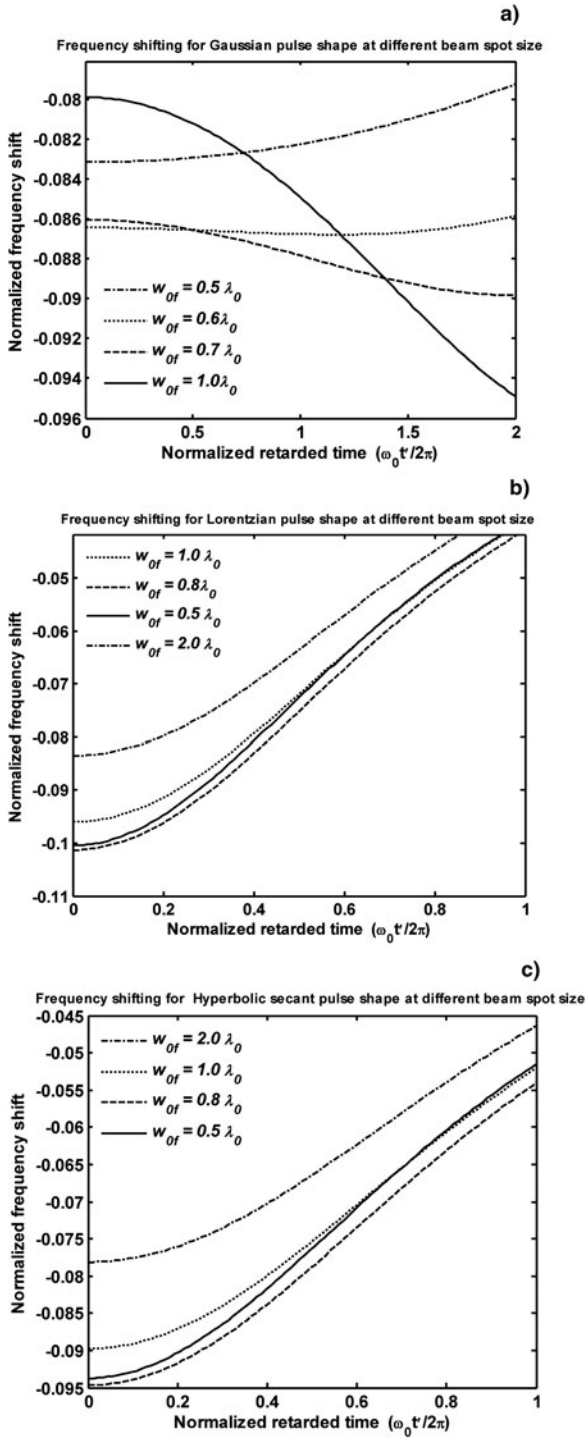

Fig. 9. Shows the variation of the axial frequency shift of a single-cycle ultrafast tightly focused TM_{01} beam as a function of retarded time, corresponding to different values of the beam spot size at the beam waist. (**a**) Gaussian, (**b**) Lorentzian, and (**c**) Hyperbolic secant pulse-shape.

https://doi.org/10.1017/S026303461100070X Published online by Cambridge University Press

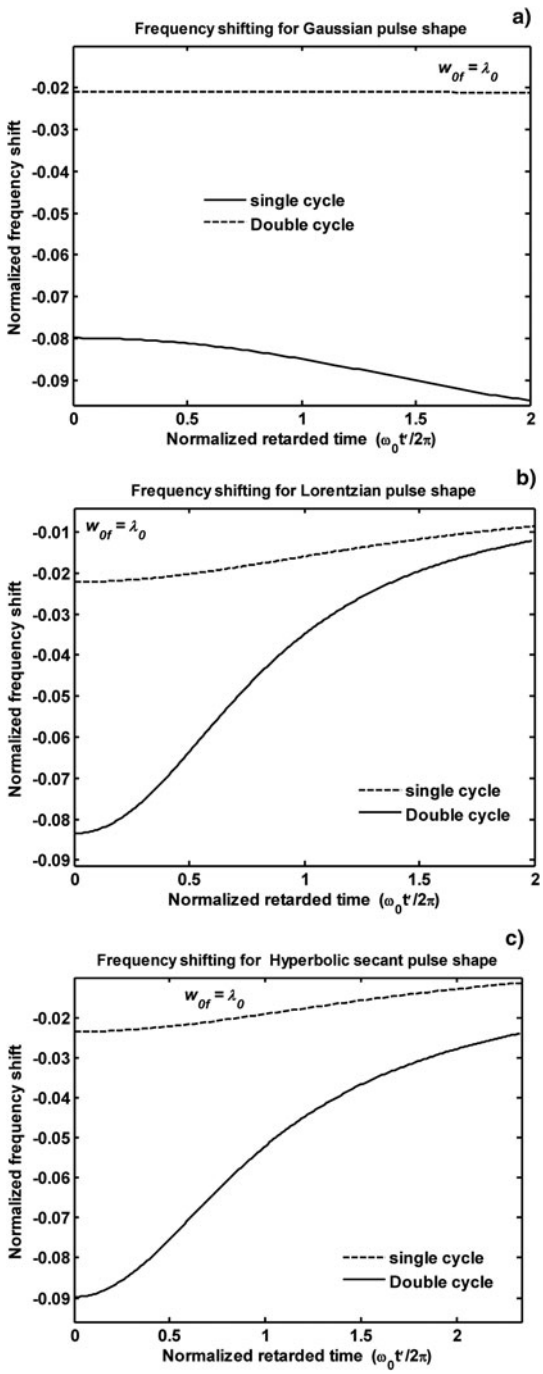

Fig. 10. Shows the temporal variation of the axial frequency-shift of an ultrafast tightly focused ($w_{0f} = \lambda_0$) TM_{01} beam, corresponding to single and double cycle in a pulse at the beam waist. (**a**) Gaussian, (**b**) Lorentzian, and (**c**) Hyperbolic secant pulse-shape.

corresponding to different values of the beam spot size. It depicts that for $0.6\lambda_0 > w_{0\lambda} > 0.25\lambda_0$ the time delay is sensitive to the pulse-shape of the single cycle laser beam. As a comparison, the magnitude of the time delay for Gaussian pulse-shape is maximum and minimum for Lorentzian pulse-shape. For bigger beam-spot-size e.g., $w_{0\lambda} > 0.6\lambda_0$, we note that these time delays are almost the same for all the temporal

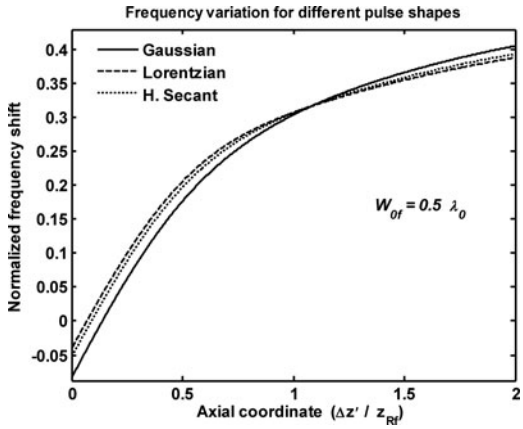

Fig. 11. Shows the pulse-shape dependence of the frequency-shift of the on-axis longitudinal electric field of a ultrafast, single-cycle tightly focused beam as a function of axial coordinate for spot size $w_{0f} = 0.5\lambda_0$, and at retarded time $t' = \tau$.

profiles of the pulse. We also observe that for spot size at the waist comparable to the wavelength, the beam of single-cycle pulse diverges more rapidly than expected from the paraxial theory.

In addition, it is also found that the frequency-shift depends on the temporal profile of the pulse, beam spot size, axial propagating distance, and also on the number of cycles in a pulse. Figure 8a, shows the variation of the axial frequency shift of an ultrafast tightly focused TM_{01} beam at the waist ($\tau = 2\pi/\omega_0$ and $w_{0f} = \lambda_0$) as a function of time. Figure 8b, represents the frequency-shift at far from the waist ($\Delta z' = \infty$). The frequency-shift at $\Delta z' = \infty$ is independent of beam-spot-size; however, it depends on the pulse-shape. It is observed from Figure 8a, that the frequency is red shifted for Gaussian, Lorentzian, and hyperbolic secant pulses. The amount of the red shift increases with time for Gaussian pulse, while it decreases for Lorentzian and hyperbolic secant pulse. The rate of decrease of

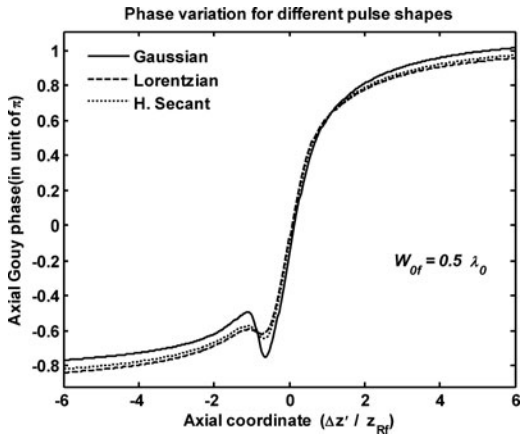

Fig. 12. Shows a comparative study of the variation of the corrected axial Gouy-phase ϕ_{GC} of the longitudinal electric field of an ultrafast, single-cycle, tightly focused ($w_{0f} = 0.5\lambda_0$) TM_{01} beam with normalized axial distance $(\Delta z'/z_{Rf})$ at retarded time $t' = \tau$.

https://doi.org/10.1017/S026303461100070X Published online by Cambridge University Press

the magnitude of red shift is more in case of the Lorentzian pulse as compared to hyperbolic secant and Gaussian pulses. It may be remarked that the variation of the red shift in case of the Gaussian pulse is found to be different from the Figure 7a of Varin *et al.* (2006). This is because an additional term $2(1.17)^2/\omega_0^2\tau^2\{1-2(1.17)^2(t')^2/\tau^2\}$ appears in the Eq. (20.1) because of the inclusion of the pulse-shape effect. In the absence of this term, the results agree with Varin *et al.* (2006). The effect of variation of the spot size on the frequency shift with retarded time is shown in Figure 9. We note that for the spot-size in the range $w_{0\lambda} \geq 0.6\lambda_0$, the amount of red frequency shift increases with retarded time for the Gaussian shape, whereas for the range $0.6\lambda_0 > w_{0\lambda} > 0.25\lambda_0$, it decreases. The effect of the number of cycles in a pulse, on the frequency shift is shown in Figure 10. It is found that in the case of single-cycle pulse, the shift in frequency is enhanced as compared to the double-cycle pulse. Figure 11, depicts the variation of the frequency shift as a function of the axial coordinate for all the three single-cycle pulses for spot size $w_{0f} = 0.5\lambda_0$ and at retarded time $t' = \tau$. It is observed from the figure that at $\Delta z'/z_{Rf} \approx 1.1$, the frequency shift is approximately same. For lower values of the axial coordinates, we get red shift whereas blue shift at higher values.

Figure 12, shows a comparative study of the variation of the corrected axial Gouy-phase ϕ_{GC} of the longitudinal electric field of Gaussian, Lorentzian, and hyperbolic secant single-cycle pulses with normalized axial distance $(\Delta z'/z_{Rf})$. From our results we observe that the Gouy phase at the Rayleigh range is independent of the pulse-shape. At a specific axial distance $\Delta z' \approx -z_{Rf}$ we get an inflexion point, and in the range $-2z_{Rf} \leq \Delta z' \leq 0$ there is a rapid change in phase which is maximum for the Gaussian pulse-shape and minimum for the Lorentzian pulse-shape.

Figure 13, represent a comparative study of the variation of the corrected axial Gouy- phase of the longitudinal electric field of Gaussian, Lorentzian, and hyperbolic secant single-cycle pulse (spot size $w_{0f} = 0.5\lambda_0$) with normalized retarded time. We see that the phase variation is maximum for Gaussian and minimum for the Lorentzian pulse shape.

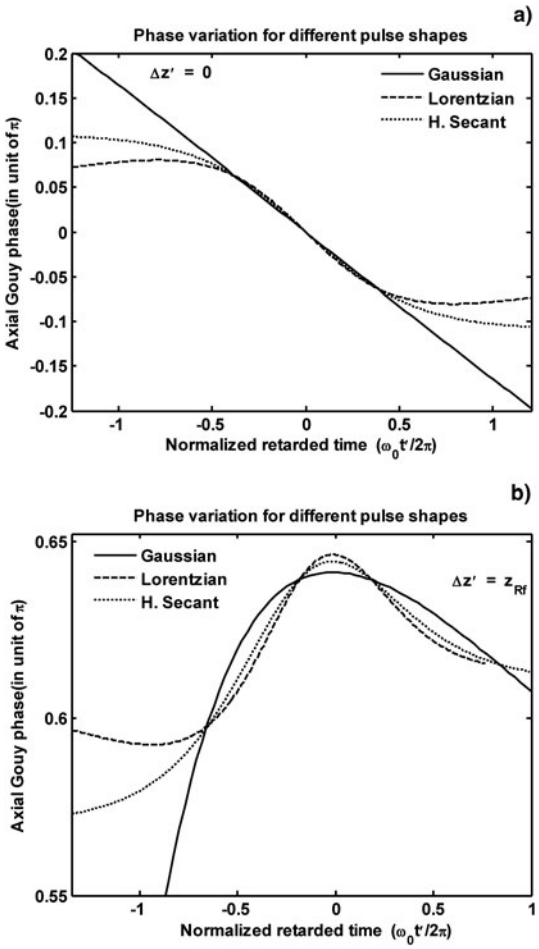

Fig. 13. Shows a comparative study of the variation of the corrected axial Gouy- phase of the longitudinal electric field of an ultrafast, single-cycle tightly focused ($w_{0f} = 0.5\lambda_0$) TM_{01} beam with normalized retarded time. (**a**) $\Delta z' = 0$ and (**b**) $\Delta z' = z_{Rf}$.

5. CONCLUSION

While estimating the strength of the longitudinal electric field of tightly focused TM_{01} laser beam in non-paraxial approximation, it is important to include the effect of the pulse-shape in addition to the number of cycles, size of the beam-spot. The evolution of the pulse envelope before the waist is faster (negative time-delay) but slowed down (positive time-delay) after the waist. This time-delay, for single-cycle pulses and for beam-spot size w_{0f} in the range $0.6\lambda_0 > w_{0f} > 0.25\lambda_0$, is pulse-shape dependent for single-cycle pulses. The carrier frequency shift and the corrected axial Gouy- phase depend on the temporal profile of the pulse, beam spot size, axial propagating distance and also on the number of cycles in a pulse.

ACKNOWLEDGMENTS

Financial support from the Department of Science & Technology, New- Delhi, (Government of India) is thankfully acknowledged. The authors are thankful to the reviewers of the paper for their valuable suggestions. The authors express thanks to Professor Naresh Dadhich, Vice-Chancellor, V. M. O. U. Kota for support and encouragement. Authors are thankful to Dr. H. B. Nandwana, Director, Science & Technology, VMOU, Kota for his kind support.

REFERENCES

Apolonski, A., Poppe, A., Tempea, G., Spielmann, Ch., Udem, Th., Holzwarth, R., Hänsch, T.W. & Krausz, F. (2000). Controlling the phase evolution of few-cycle light pulses. *Phys. Rev. Lett.* **85**, 740–743.

Baeva, T., Gordienko, S. & Pukhov, A. (2006). Theory of high-order harmonic generation in relativistic laser interaction with over dense plasma. *Phys. Rev. E* **74**, 046404/1–11.

https://doi.org/10.1017/S026303461100070X Published online by Cambridge University Press

Brabec, T. & Krausz, F. (1997). Nonlinear optical pulse propagation in the single-cycle regime. *Phys. Rev. Lett*. **78**, 3282–3285.

Brabec, T. & Krausz, F. (2000). Intense few-cycle laser fields: Frontier of nonlinear optics. *Rev. Mod. Phys*. **72**, 545–591.

Corkum, P.B. & Krausz, F. (2007). Attosecond science. *Nat. Phys*. **3**, 281–287.

Dorn, R., Quabis, S. & Leuchs, G. (2003). Sharper focus for a radially polarized light beam. *Phys. Rev. Lett*. **91**, 23390/1–4.

Dromey, B., Kar, S., Bellei, C., Carroll, D.C., Clarke, R.J., Green, J.S., Kneip, S., Markey, K., Nagel, S.R., Simpson, P.T., Willingale, L., Mckenna, P., Neely, D., Najmudin, Z., Krushelnick, K., Norreys, P. A. & Zepf, M. (2007). Bright multi-KeV harmonic generation from relativistically oscillating plasma surfaces. *Phys. Rev. Lett*. **99**, 0850011/1–14.

Dromey, B., Rykovanov, S.G., Adams, D., Hörlein, R., Nomura, Y., Carroll, D.C., Foster, P.S., Kar, S., Markey, K., Mckenna, P., Neely, D., Geissler, M., Tsakiris, G.D. & Zepf, M. (2009). Tunable enhancement of high harmonic emission from laser solid interactions. *Phys. Rev. Lett*. **102**, 225002/1–4.

Esarey, E., Scchroeder, C.B. & Leemans, W.P. (2009). Physics of laser-driven plasma–based electron accelerators. *Rev. Mod. Phys*. **81**, 1229–1285.

Gupta, M.K., Sharma, R.P. & Mahmoud, S.T. (2007). Generation of plasma wave and third harmonic generation at ultra relativistic laser power. *Laser Part. Beams* **25**, 211–218.

Krausz, F. & Ivanov, M. (2009). Attosecond physics. *Rev. Mod. Phys*. **81**, 163–234.

Kröll, J., Darmo, J., Dhillon, S.S., Marcadet, X., Calligaro, M., Sirtori, C. & Unterrainer, K. (2007). Phase- resolved measurements of stimulated emission in a laser. *Nat. Lett*. **449**, 698–701.

Lichters, R., Meyer-Ter-Vehn, J. & Pukhov, A. (1996). Short-pulse laser harmonics from oscillating plasma surfaces driven at relativistic intensity. *Phys. Plasmas* **3**, 3425–3437.

Malav, H., Maheshwari, K.P. & Choyal, Y. (2011*b*). Analytical and numerical investigation of pulse-shape effect on the interaction of an ultrashort, intense, few-cycle laser pulse with a thin plasma layer. *Laser Part. Beams* **29**, 45–54.

Malav, H., Maheshwari, K.P. & Senecha, V. (2011*a*). Analytical and numerical investigation of the effect of pulse shape of intense, few-cycle TM_{01} laser on the acceleration of charged particles. *Indian J. Pure Appl.Phys*. **49**, 251–256.

Malav, H., Maheshwari, K.P., Meghwal, R.S., Choyal, Y. & Sharma, R. (2010). Analytical and numerical investigation of diffraction effects on the nonlinear propagation of ultra-intense few-cycle optical pulses in plasmas. *J. Plasma Phys*. **76**, 209–227.

Nisoli, M., Sansone, G., Stagira, S., Silvestri, S.D., Vozzi, C., Pascolini, M., Poletto, L., Villoresi, P. & Tondello, G. (2003). Effects of carrier-envelope phase differences of few-optical-cycle light pulses in single-shot high- order-harmonic spectra. *Phys. Rev. Letters* **91**, 2139051/1–54.

Paulus, G.G., Lindner, F., Walther, H., Baltuška, A., Gouliemakis, E., Lezius, M. & Krausz, F. (2003). Measurement of the phase of few-cycle laser pulses. *Phys. Rev. Lett*. **91**, 253004 (1–4).

Porras, M.A. (2001). Pulse correction to monochromatic light-beam propagation. *Opt. Lett*. **26**, 44–46.

Porras, M.A. (2002). Diffraction effects in few-cycle optical pulses., *Phys. Rev. E* **65**, 026606/1–11.

Porras, M.A. (2009). Characterization of the electric field of focused pulsed Gaussian beams for phase –sensitive interactions with matter. *Opt. Lett*. **34**, 1546–1548.

Schenkel, B., Biegert, J., Keller, U., Vozzi, C., Nisoli, M., Sansone, G., Stagira, S., De Silvestri, S., & Svelto, O. (2003). Generation of 3.8-fs pulses from adaptive compression of a cascaded hollow fiber supercontinuum. *Opt. Lett*. **28**, 1987–1989.

Sprangle, P., Hafizi, B., Penano, J.R., Hubbard, R.F., Ting, A., Zigler, A. & Antonsen, T.M. (2000). Stable laser-pulse propagation in plasma channels for GeV electron acceleration. *Phys. Rev. Lett*. **85**, 5110–5113.

Varin, C. & Piché, M. (2002). Acceleration of ultra-relativistic electrons using high-intensity TM_{01} laser beams. *Appl. Phys. B* **74**, S83–S88.

Varin, C., Piché, M. & Porras, M.A. (2005). Acceleration of electron from rest to GeV energies by ultrashort transverse magnetic laser pulses in free space. *Phys. Rev. E* **71**, 026603/1–10.

Varin, C., Piché, M. & Porras, M.A. (2006). Analytical calculation of the longitudinal electric field resulting from the tight focusing of an ultrafast transverse-magnetic laser beam. *J. Opt. Soc. Am. A* **23**, 2027–2038.

Varro, S. (2007). Linear and nonlinear absolute phase effects in interactions of ultrashort laser pulses with a metal nano-layer or with a thin plasma layer. *Laser part. Beams* **25**, 379–390.

Villoresi, P., Barbiero, P., Poletto, L., Nisoli, M., Cerullo, G., Priori, E., Stagira, S., Lisco, C. De, Bruzzese, R. & Altucci, C. (2001). Study of few-optical-cycles generation of high-order harmonics. *Laser Part. Beams* **19**, 41–45.

Wittmann, T., Horvath, B., Helml, W., Schätzel, M.G., Gu, X., Cavalieri, A.L., Paulus, G.G. & Kienberger, R. (2009). Single-shot carrier-envelope phase measurement of few-cycle laser pulses. *Nat. Phys*. **5**, 357–362.

https://doi.org/10.1017/S026303461100070X Published online by Cambridge University Press